CCFE
CULHAM CENTRE FOR FUSION ENERGY

UK Atomic Energy Authority

UKAEA-CCFE-PR(24)187

Hyun-Tae Kim, F. Auriemma, K. Kirov, Z. Stancar, R. Lorenzini, J. Ferreira, P. Huynh, S. Gabriellini, M. Poradzinski, D. Gallart, M. Nocente, L. Garzotti, C. Maggi, M. Maslov, F. Casson, A. Di. Sienna, J. Citrin, P. Strand, R. Gatto, E. Tholerus, E. Belli, R. Sharma, A. Osipov, E. Fransson, A. Kappatou, C. D. Challis, E. Lerche, D. Ester, J. Garcia, JET contributors

Validation of DT fusion power prediction capability against 2021 JET DT experiments

Validation of DT fusion power prediction capability against 2021 JET DT experiments

Hyun-Tae Kim, F. Auriemma, K. Kirov, Z. Stancar, R. Lorenzini, J. Ferreira, P. Huynh, S. Gabriellini, M. Poradzinski, D. Gallart, M. Nocente, L. Garzotti, C. Maggi, M. Maslov, F. Casson, A. Di. Sienna, J. Citrin, P. Strand, R. Gatto, E. Tholerus, E. Belli, R. Sharma, A. Osipov, E. Fransson, A. Kappatou, C. D. Challis, E. Lerche, D. Eester, J. Garcia, JET contributors

This is a preprint of a paper submitted for publication in Nuclear Fusion

Validation of DT fusion power prediction capability against 2021 JET DT experiments

February 17, 2023

Hyun-Tae Kim[1], Fulvio Auriemma[2], Jorge Ferreira[3], Stefano Gabriellini[4], Aaron Ho[5], Philippe Huynh[6], Krassimir Kirov[1], Rita Lorenzini[2], Michele Marin[7], Michal Poradzinski[1], Nan Shi[8], Gary Staebler[8], Ziga Stancar[1], Gediminas Stankunas[9], Vito Konrad Zotta[4], Emily Belli[8], Francis J Casson[1], Clive D Challis[1], Jonathan Citrin[5], Dirk van Eester[10], Emil Fransson[11], Daniel Gallart[12], Jeronimo Garcia[6], Luca Garzotti[1], Renato Gatto[4], Joerg Hobirk[13], Athina Kappatou[13], Ernesto Lerche[10], Andrei Ludvig-Osipov[11] Costanza Maggi[1], Mikhail Maslov[1], Massimo Nocente[14], Ridhima Sharma[1], Alessandro Di Siena[13], Par Strand[11], Emmi Tholerus [1], Dimitriy Yadykin[11] and JET contributors

[1] UKAEA, Abingdon, United Kingdom
[2] Consorzio RFX, corso Stati Uniti, 4, Padova, 35127, ITALY
[3] Instituto de Plasmas e Fusão Nuclear, Instituto Superior Técnico, Universidade de Lisboa, 1049-001 Lisboa, Portugal
[4] Sapienza University of Rome, Rome, Italy
[5] Dutch Institute for Fundamental Energy Research (DIFFER), PO Box 6336, 5600 HH Eindhoven, Netherlands
[6] IRFM, CEA F-13108, Sant-Paul-lez-Durance, France
[7] SPC, Swiss Plasma Center, Ecole Polytechnique Federale de Lausanne, Station 13, Lausanne, 1015, Switzerland
[8] General Atomics, PO Box 85608, San Diego, CA 92186-5608, United States of America
[9] Lithuanian Energy Institute, Laboratory of Nuclear Installation Safety, Breslaujos Str. 3, LT-44403, Kaunas, Lithuania
[10] LPP-ERM/KMS, Association EUROFUSION-Belgian State, TEC partner, Brussels, Belgium
[11] Department of Space, Earth and Environment, Chalmers University of Technology, Gothenburg, Sweden
[12] Barcelona Supercomputer Center, Barcelona, Spain
[13] Max-Planck Institut für Plasmaphysik Garching, Germany
[14] Department of Physics "G. Occhialini," University of Milano-Bicocca, 20126 Milan, Italy

Hyun-Tae.Kim@ukaea.uk

Abstract

JET experiments using the fuel mixture envisaged for fusion power plants, deuterium and tritium (D-T), provide a unique opportunity to validate existing D-T fusion power prediction capabilities in support of future device design and operation preparation. The 2021 JET D-T experimental campaign has achieved D-T fusion powers sustained over 5 seconds in ITER-relevant conditions[1] i.e. operation with the baseline or hybrid scenario in the full metallic wall. In preparation of the 2021 JET D-T experimental campaign, extensive DT predictive modelling was carried out with several assumptions based on D discharges[2]. To improve the validity of ITER D-T predictive modelling in the future, it is important to use the input data measured from 2021 JET D-T discharges in the core predictive modelling, and to specify the accuracy of the DT fusion power prediction in comparison with the experiments. This paper reports on the validation of the core integrated modelling with TRANSP, JINTRAC, and ETS coupled with a quasilinear turbulent transport model (TGLF or QualLiKiz) against the measured data in 2021 JET DT discharges. Detailed simulation settings and the heating and transport models used are described.

The DT fusion power calculated with the interpretive TRANSP runs for 38 DT discharges (12 baseline and 26 hybrid discharges) reproduced the measured values within 20%. This indicates the additional uncertainties, that could result from the measurement error bars in kinetic profiles, impurity contents and neutron rates, and also from the beam-thermal fusion reaction modelling, are less than 20% in total. The good statistical agreement confirms that we have the capability to accurately calculate the D-T fusion power if correct kinetic profiles are predicted, and indicates that any larger deviation of the DT fusion power prediction from the measured fusion power could be attributed to the deviation of the predicted kinetic profiles from the measured kinetic profiles in these plasma scenarios. Without any posterior adjustment of the simulation settings, the ratio of predicted DT fusion power to the measured fusion power was found as $65\% - 96\%$ for the DT baseline and $79\% - 97\%$ for DT hybrid discharge. Possible reasons for the lower DT prediction are discussed and future works to improve the fusion power prediction capability are suggested.

The DT predictive modelling results have also been compared to the predictive modelling of the counterpart D discharges, where the key engineering parameters are similar. Features in the predicted kinetic profiles of DT discharges such as underprediction of n_e are also found in the prediction results of the counterpart D discharges, and it leads to similar levels of the normalized neutron rate prediction between the modelling results of DT and the counterpart D discharges. This implies that the credibility of DT fusion power prediction could be a priori estimated by the prediction quality of the preparatory D discharges, which will be attempted before actual DT experiments.

1 Introduction

Reliable DT fusion power prediction is important to optimize DT operation scenarios and to design future DT fusion reactors. Predicting fusion power is a challenging task as it is very sensitive to key plasma parameters. Thermal DT fusion reaction rate scales faster than a linear increase with fuel ion density and temperature. It thus requires sophisticated integrated modelling that correctly predicts the key plasma parameters by modelling the heating and transport in a plasma. To ensure trustworthy prediction, it is essential to quantitatively assess the present prediction modelling tools using existing experimental data and to identify improvements required in the prediction models. Such a validation, nevertheless, has not been possible until now due to the lack of DT experimental data in present devices. The previous DT experimental campaign was in 1997 at JET[3]. The objectives in most DT discharges at that time were, however, to produce transient high performance pulses, which were

operated with ELM-free H-mode regime or optimized shear regimes. Such transient discharges are not directly relevant to ITER DT discharges, where stationary operation is one of the key objectives. Although there were a small number of stationary H-mode discharges in 1997 [4], the quality of experimental data is not good enough to quantatively validate the predictive modelling. Furthermore, all the DT discharges in 1997 were operated with the carbon plasma facing components.

ITER is designed to have a full metallic wall (i.e. beryllium first wall and tungsten divertor). In 2011 the previous carbon wall in JET was replaced with an ITER-like full metallic wall to produce a similar environment surrounding the plasma as ITER [5]. It has been reported in JET and ASDEX-U that the plasma energy confinement is affected by the presence of a metal wall[6]. Since the wall refurbishment, plasma operations with the ITER-like wall have been extensively explored [7, 8, 9] and demonstrated the two main operation scenarios envisaged in ITER (baseline and hybrid scenarios). The baseline scenario pursues high plasma performance at high I_p and B_T, and relaxed J_p profiles ($\beta_N - 1.8$, $q_{95} - 3$) [7]. On the other hand, the hybrid scenario takes the advantages of the favourable confinement behaviour when operating at high β_N and the possibility to avoid performance degrading MHD with a tailored J_p profiles and $q_0 > 1$ ($\beta_N = 2 - 3$, $q_{95} - 4.8$) [10]. With the optimized operation scenarios, EURO*fusion* performed the second JET DT experimental campaign in 2021 [1].

The 2021 JET DT experimental campaign achieved DT fusion power sustained over 5 seconds in the ITER-relevant conditions [1]. Since no further DT experimental campaign is foreseen in any other ITER partner's present devices before ITER DT experiments planned in the 2030s, 2021 JET DT experimental campaign has provided a unique opportunity to validate the present DT fusion power prediction capability before ITER DT experiments take place. To provide the scientific validity of ITER DT predictive modelling, it is important to document the models and simulation settings used in the predictive integrated modelling of 2021 JET DT discharges, and to specify the accuracy of DT fusion power predictions to the measured values. It has motivated collective modelling activities organized in *JET DT scenario extrapolation task*, and considerable effort was devoted to interpretive and predictive modelling of the achieved high performance DT plasmas [11, 12, 13, 14].

There are several integrated modelling codes actively used in the fusion community (e.g. TRANSP[15, 16], JINTRAC[17], and ETS[18]) that can predict the kinetic profiles and the fast particle population. Each code uses different heating and transport models, which will be introduced in section 3.2. In addition, even the numerical algorithm to solve the energy and particle balance equations in the integrated modelling codes are also not identical [19]. For example, TRANSP solves the equation for electron particle balance (and ion particle densities are calculated with the quasi-neutrality assumption), while JINTRAC and ETS solves the equation for each ion particle balance (and electron particle density is calculated with the quasi-neutrality assumption) [19]. These differences could cause different fusion power predictions. To address the uncertainty resulting from the choice of modelling codes, DT fusion power has been computed with the three mainstream integrated modelling codes, which are coupled to the two quasilinear turbulent transport models, TGLF or QuaLiKiz (i.e. TRANSP-TGLF, JINTRAC-TGLF, JINTRAC-QuaLiKiz, and ETS-TGLF). Using identical input data and standard simulation settings, the integrated modelling codes simulated the best performing D-T baseline and hybrid discharges from the 2021 JET D-T campaign. The predicted D-T fusion powers were compared between codes and with the measured fusion power.

In order to improve the chance of success in the D-T experimental campaign, it was necessary to optimise the planned operational scenarios using D discharges during the previous years [20], using

predictive modelling to guide the experiments [2]. Similarly, ITER D-T operational scenarios need to be developed with D discharges beforehand, with intensive D-T discharge predictive modelling based on the achieved D discharges. An important question is whether the quality of predictive modelling of preparatory D discharges (i.e. how well they predict the kinetic profiles and the neuron rates) can be used as a good indicator of the D-T discharges prediction quality, and in particular whether features of D predictive modelling are also apparent in the D-T predictive modelling. This motivated attempts to correlate the prediction quality of D discharges with that for the 2021 campaign D-T discharges. D discharges with the engineering parameters, which are similar to the high fusion power baseline and hybrid D-T discharges, were selected, and their predictive integrated modelling results were compared to the D-T discharge modelling results.

This paper is structured as follows in order to outline the validation of current DT fusion power prediction capability. In section 2, to assess uncertainties of fusion power prediction separately from the kinetic profile prediction, DT fusion power calculated with interpretive TRANSP runs are statistically compared to the measured values. In section 3.1, two high performance baseline DT discharges (i.e. baseline and hybrid) and their counterpart D discharges that were used for predictive integrated modelling are introduced. In section 3.2, the predictive integrated modelling codes are introduced together with description of the heating and trasnport models. In section 3.3, the DT fusion power prediction results are presented, together with the modelling results of kinetic profiles and the heat and particle source profiles. Uncertainties in the predicted fusion power and future works are suggested in section 3.4. Section 4 provides conclusion.

2 DT fusion power calculation with interpretive integrated modelling

DT fusion power is a function of multiple parameters. In principle, it can be calculated with the following formula:

$$\begin{aligned} P_{fus}[MW] = \Big(& \int n_{th,D} n_{th,T} < \sigma v > (T_D, T_T) dV \\ & + \int n_{th,D} n_{fast,T} < \sigma v > (T_D, E_{fast,T}) dV \\ & + \int n_{th,T} n_{fast,D} < \sigma v > (T_T, E_{fast,D}) dV \\ & + \int n_{fast,D} n_{fast,T} < \sigma v > (E_{fast,D}, E_{fast,T}) dV \Big) \times 17.6 \times 1.6 \times 10^{-19} \end{aligned} \tag{1}$$

Where n_{th} and n_{fast} are the thermal and the NBI fast ion density, T_D and T_T are the temperature of D and T thermal ions, and E_{fast} is the fast ion energy. $17.6 \times 1.6 \times 10^{-19}$ is the fusion energy per DT fusion reaction in the unit of $[MJ]$. In equation (1) the first term is the thermonuclear fusion power, the second and the third terms are the beam-thermal fusion power, and the last term is the beam-beam fusion power. The first term is only a function of ion temperature and density, while the other terms require NBI heating models (and ICRF heating models to simulate fast ion acceleration by RF wave), which simulate the slowing-down process of fast ions. The fourth term is typically much smaller than the other terms, and in most JET discharges it is small enough to ignore.

As can be seen in equation (1), fusion power calculation requires integrated modelling, which involves the fusion cross sections and several physics models e.g. NBI heating, ICRF heating, turbulent transport, fast ion population, and equilibrium, which are functions of kinetic profiles. Interpretive TRANSP runs calculate the fusion power with prescribed kinetic profiles (i.e. measured ion temperature and inferred ion density from measured n_e) and the internal NBI heating model i.e. NUBEAM [23][24]. Use of measured kinetic profiles is the main difference compared to the predictive modelling, where the fusion power is calculated with the predicted kinetic profiles. Even with measured kinetic profiles, fusion power calculation in the interpretive simulations could have additional uncertainties due to the measurement error bars in kinetic profiles, impurity content and neutron rate, and the calculation error bars in the beam-thermal fusion reaction modelling. To estimate these uncertainties, interpretive TRANSP runs have been performed for 12 baseline ($I_p = 3.0 - 3.5[MA]$, $B_T = 2.8 - 3.3[T]$, $P_{NBI} = 23 - 28.7[MW]$, and $P_{ICRF} = 1.6 - 3.9[MW]$) and 26 hybrid discharges ($I_p = 2.3[MA]$, $B_T = 3.4[T]$, $P_{NBI} = 19.7 - 29.1[MW]$, and $P_{ICRF} = 1.2 - 4.7[MW]$), which were selected based on the good diagnostics data. The ratio of fuel gas mixture in the discharges was measured to be about $50\%D$ and $50\%T$ mixture with edge H,D,T-alpha spectroscopy. The initial ratio of the fuel ion mixture in the interpretive TRANSP runs was assumed with the measured data, and the slight evolution of D and T ion ratio due to the NBI beam fuelling was consistently calculated in the interpretive TRANSP. Figure 1(a) shows the moderate range of the NBI and ICRF heating power in the discharges, and Table 4 in Appendix A lists the shot numbers, operation scenarios, and time windows in each discharge. The interpretive TRANSP runs were made with a standard simulation setting and a common procedure for experimental input data preparation. The details of the interpretive TRANSP runs and modelling redsults with a wider range of discharges (e.g. different RF scheme, T-rich discharges) can be found in [21, 22]. Figure 1(b) shows that all of the fusion power calculated in the 38 DT discharges are located within 20% error bars to the measured values. This indicates that with prescribed kinetic profiles the fusion power can be modelled to within an accuracy of 20%.

Figure 2(a)(b) shows the thermonuclear fusion power and the beam-thermal fusion power, calculated in the interpretive TRANSP simulations. At the same total fusion power, the baseline discharges have higher thermonuclear fusion power than the hybrid discharges, and vice versa for the beam-thermal fusion power. This is due to the higher ion density in the baseline discharges, which is a typical feature of the high I_p operation. In both high performance DT baseline and hybrid discharges, the increase in the total fusion power was mainly driven by the increase in the NBI heating power, with the beam-thermal fusion power and thermonuclear fusion power both increasing with NBI heating. Since the latter increases more rapidly, the ratio of the thermonuclear fusion power to the total fusion power increases with the total fusion power in both scenarios (see figure 2(c)). The highest thermonuclear contribution to the total fusion yield of more than 50% was observed in the highest performing baseline discharges. This suggests that the thermonuclear contribution should be dominant in the higher performance baseline or hybrid operation regime, planned in ITER.

NUBEAM in TRANSP, which will be introduced more in detail in the next section, simulates the slowing down of the alpha particles with the Monte-Carlo method using the same approach as for the NBI ions. Figure 2(d) shows the alpha heating to ions calculated in the interpretive TRANSP simulations. The calculated alpha heating power to ions linearly increases with the total fusion power. However, the amount of the alpha heating is very small (i.e. < 0.25MW) and thus is unlikely to have any significant effects on T_i profiles, though the alpha heating is modelled in the predictive integrated

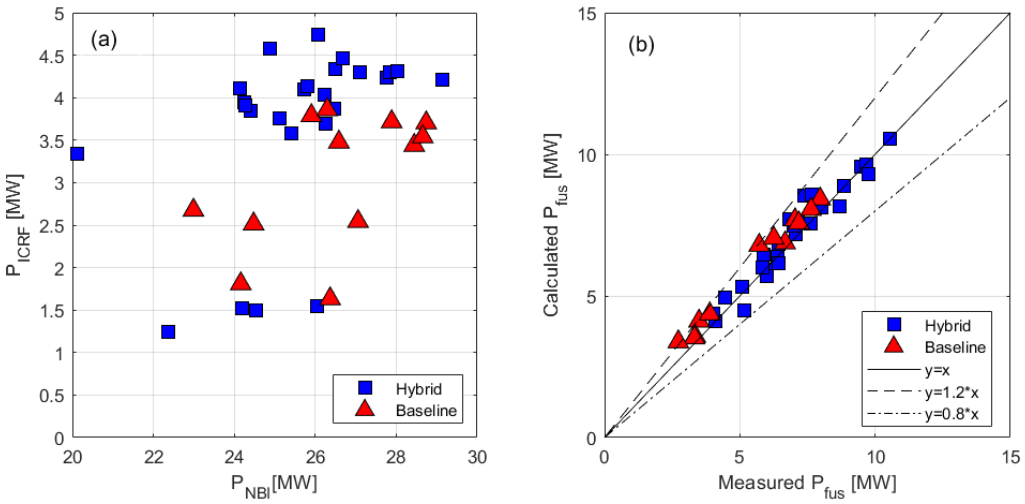

Figure 1: (a)NBI and ICRF heating power in the database (b)DT fusion power calculation with interpretive TRANSP for JET DTE2 discharges[21, 22]

modelling in this paper.

3 DT fusion power calculation with predictive integrated modelling

3.1 Reference discharges

In preparation for JET DT operation, the baseline and hybrid scenarios were extensively explored to optimize the operation with D discharges in the previous years [7, 9], and the optimized scenarios successfully demonstrated high performance DT discharges with the ITER-Like wall in 2021. Among the achieved DT discharges, the reference baseline and hybrid DT discharges which have 50%-50% D-T fuel mixture, a stationary time window, and high fusion performance were selected for predictive integrated modelling, aiming to assess our current fusion power prediction capability for ITER-relevant DT discharges. The shot numbers and operation parameters are indicated in Table 1.

The preparatory D discharges were also selected for comparison with the DT discharges. The gold and blue lines in figure 3 are the time traces in the reference DT discharges and the counterpart D discharges, respectively. As can be seen, the key engineering parameters such as I_p, B_T, the total heating power (i.e. $P_{NBI} + P_{ICRF} + P_\alpha$) are similar in the DT and D counterpart discharges.[1] The experimental data (e.g. pedestal values of T_i, T_e, and n_e) in the reference discharges were used as boundary conditions in the integrated transport modelling codes to calculate the kinitic profiles in the core ($0 \leq \rho \leq 0.85$), and the corresponding fusion power.

One of the main differences between the baseline and the hybrid discharge operation is the gas

[1]Note, there are counterpart hybrid DT discharges with more similar engingeering parameters were achieved in 2022 Aug, when the modelling work in this paper has been almost finished. The discharges were introduced in [10].

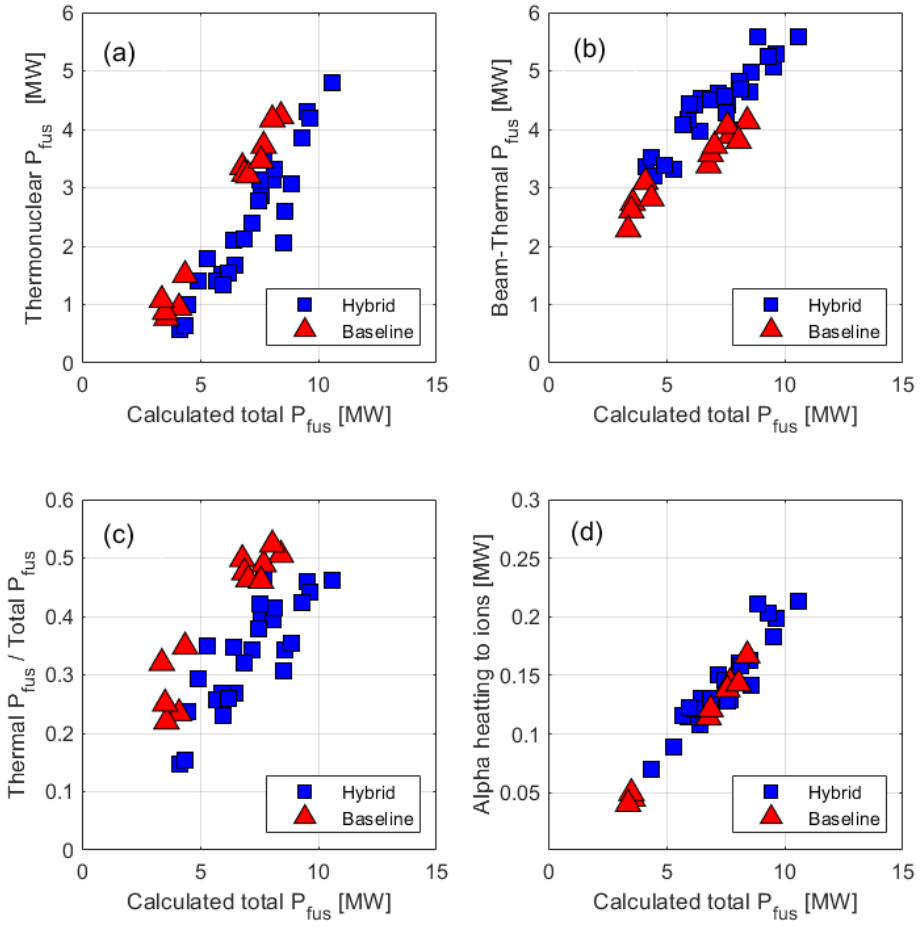

Figure 2: (a)The thermonuclear fusion power (b)the Beam-thermal fusion power, (c)the ratio of the thermal neutron rate to the total neutron rate, and (b) Alpha heating power to ions, calculated in the interpretive TRANSP.

Operation scenario	**Baseline D**	**Baseline DT**	**Hybrid D**	**Hybrid DT**
Shot number	96482	99948	97781	99949
Time window [sec]	$50.0 - 50.5$	$49.5 - 50$	$49.0 - 49.5$	$48.75 - 49.25$
D and T ratio	100 % and 0%	49% and 51%	100% and 0%	47% and 53%
$I_p[MA]$	3.5	3.5	2.3	2.3
$B_T[T]$	3.3	3.3	3.4	3.4
q_{95}	3.2	3.2	4.8	4.8
$P_{NBI}[MW]$	29.5	28.7	30	27
$P_{ICRF}[MW]$	4.9	3.6	2.9	4.2
$P_\alpha[MW]$	0	1.5	0	1.25
ICRF scheme	H at N=1 (dipole phasing)	H at N=1 (dipole phasing)	H at N=1 (dipole phasing)	H at N=1 (dipole phasing)
H minority fraction ($=H/(H+D+T)$)	4%	2%	3%	4%
Fuelling	D gas injection + D ELM pacing pellet	DT gas injection + D ELM pacing pellet	D gas injection	DT gas injection
Neutron rate [$\times 10^{18}\#/sec$]	0.025	3	0.035	2.5

Table 1: Values of the time traces averaged over the analysis time window in the reference DT discharges for predictive integrated modelling

fuelling scheme. For ELM frequency control, the baseline DT discharges require D ELM pacing pellets[2] in addition to DT gas injection [25] whereas the hybrid discharges can maintain stable type-I ELM with DT gas injection only. During the scenario optimization in previous years, it was found that low gas fuelling improves the ion heat confinement, allowing high fusion performance [8, 26]. However, low gas injection in the baseline discharges reduces the ELM frequency, increasing the risk of tungsten accumulation, thereby leading to disruption. Low gas operation in the baseline discharges was only possible when sufficient ELM frequency was maintained by using ELM pacing pellets.

The time windows for DT fusion power prediction modelling have been selected to be $49.5 - 50$ seconds in shot number 99948 (DT) and $48.75 - 49.25$ seconds in 99949 (DT), as they have the most stable maximum fusion performances in the discharges, which are $8.3MW$ and $7.2MW$, respectively. As can be seen by the time traces of core T_e and n_e in Figure 3, both time windows have approximately stationary plasma parameters. It should be, however, noted that 99948 (DT) exhibits a gradual increase in core n_e. It resulted from the increase in the pedestal n_e due to the intermittency of ELM events, despite the use of ELM pacing pellets. The reduced ELM frequency led to reduced tungsten flushing and excessive radiation at the low field side, thereby terminating the discharge at 51.4 seconds.

Stationary time windows of the counterpart D discharges were selected to be 50.0 - 50.5 seconds in 96482 (D) and 49.0 - 49.5 seconds in 97781 (D), respectively. Figure 4 compares the measured kinetic

[2]T pellets are not available to use for a technical reason.

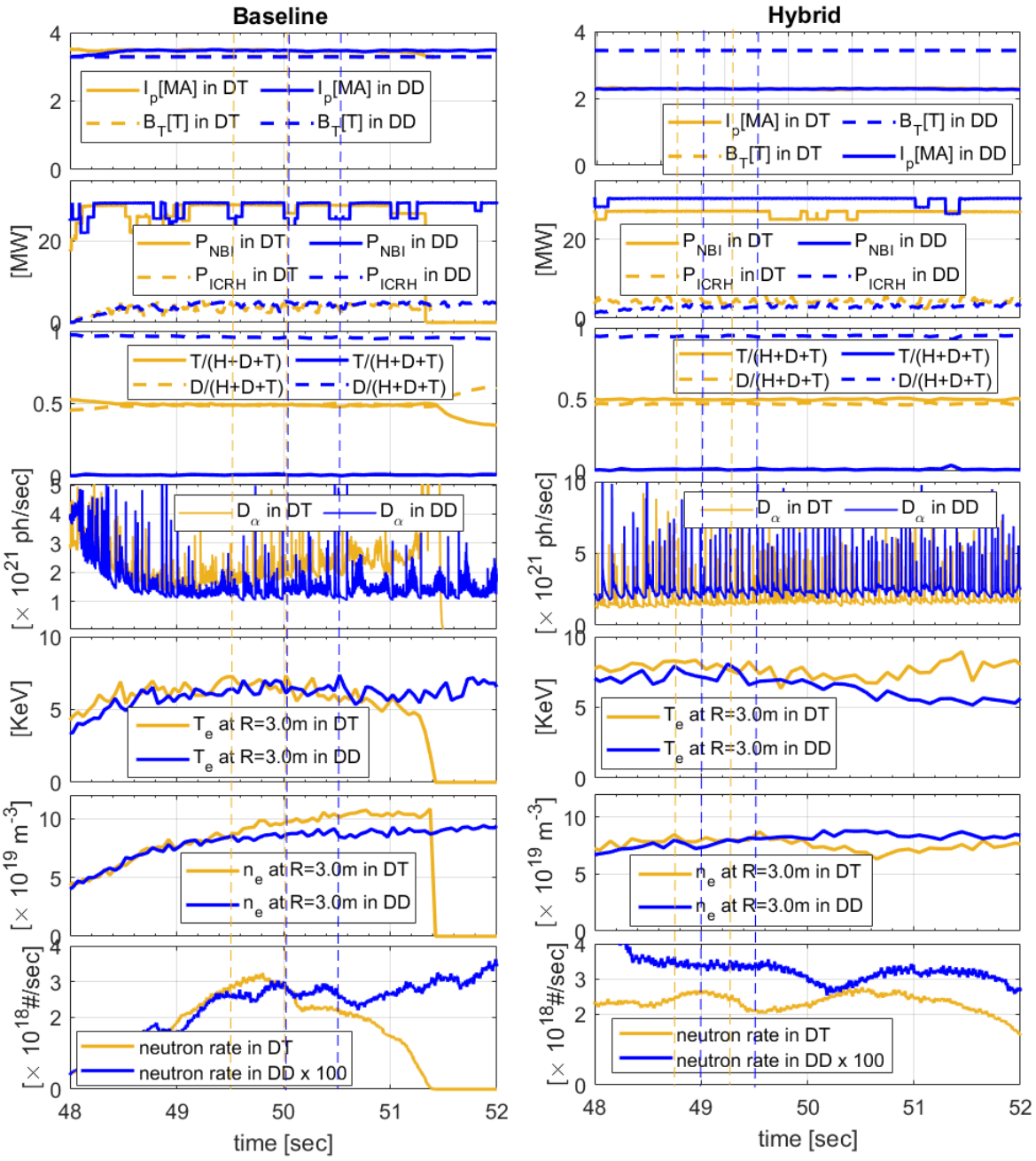

Figure 3: Time traces of reference baseline ($50\% - 50\%$ DT 99948 and the counterpart 100 % D 96482) and hybrid discharges (100 % D 97781 and $50\% - 50\%$ DT 99949). Time windows that were used for predictive modelling have been indicated by vertical dashed lines (gold dashed lines for DT and blue dashed lines for D).

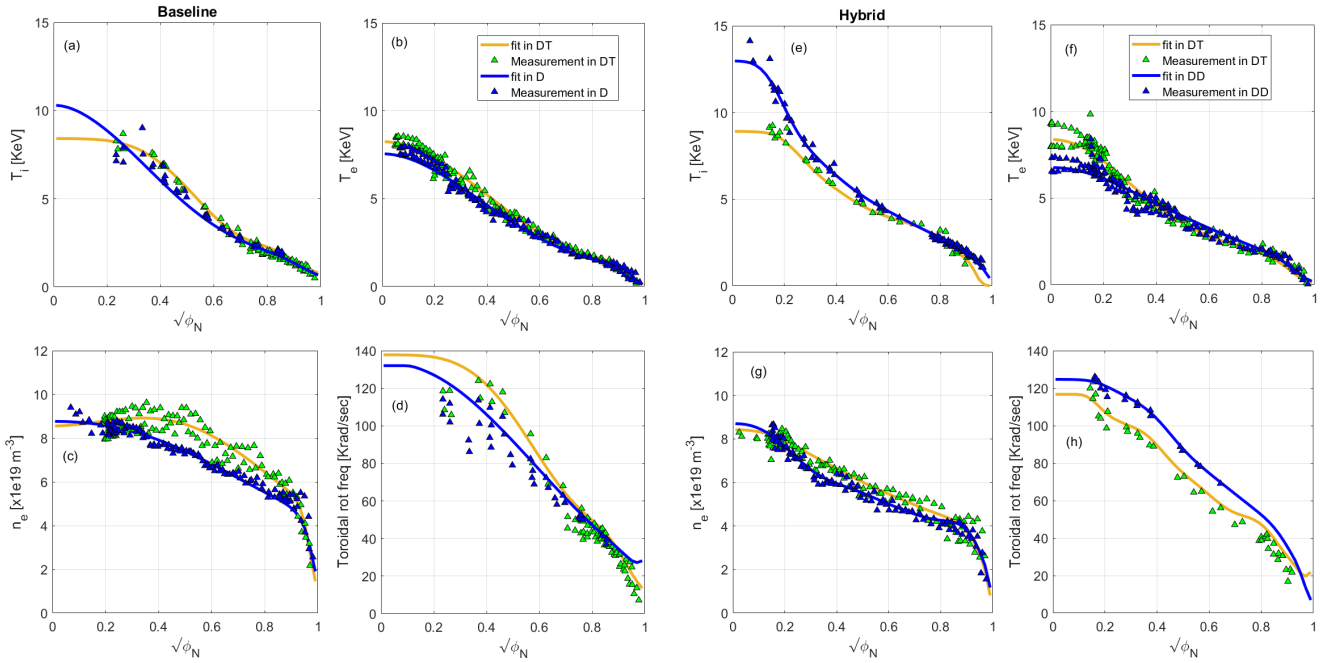

Figure 4: Measured kinetic profiles of the reference baseline (averaged over 49.5 - 50.0 seconds in 50% − 50% DT 99948 and 50.0 - 50.5 seconds in the counterpart 100 % D 96482) and hybrid discharges (averaged over 48.75 - 49.25 seconds in 50% − 50% DT 99949 and 49.0 - 49.5 seconds in 100 % D 97781). T_e and n_e are measured by Thomson scattering and T_i and the rotation frequency are measured by Charge Exchange Radiation spectroscopy.

profiles between the DT (gold) and D (blue) counterpart discharges. In the baseline discharges, the major difference is the pedestal n_e. 99948 (DT) has a higher pedestal n_e than 96482 (D), leading to a higher n_e for a wide radial region in the core. In the hybrid discharges, T_i within $\rho \leq 0.2$ is higher in 97781 (D) than in 99949 (DT). This could be due to the deeper penetration of D NBI beams than of T NBI beam, as D NBI beams have a higher speed than T NBI beams at the given NBI voltages. The NBI heat and particle deposition calculated with the interpretive TRANSP runs also consistently shows the higher core deposition in 97781 (D) (see figure 9).

3.2 Predictive integrated modelling codes

3.2.1 Common input and simulation settings

Three integrated modelling codes TRANSP [15, 16], JINTRAC [17], and ETS [18], which have been used as the major tools in EURO*fusion* integrated modelling activities, were selected to evaluate the present DT fusion power prediction capability and to assess the uncertainty that could result from the choice of modelling tools. Also, TGYRO developed in General Atomics has participated in the collective modelling to cross-benchmrk with TRANSP, as the heat and particle source profile data in TGYRO are prescribed by interpretive TRANSP data and the same transport model (i.e. TGLF) is used.

To assess the fusion power prediction capability, a standard simulation setting and an identical set of input data were used in all integrated modelling codes (TRANSP-TGLF, JINTRAC-TGLF, JINTRAC-QuaLiKiz, ETS-TGLF, and TGYRO-TGLF), without any posterior adjustment of simulation settings trying to match with experimental data. Table 2 lists the simulation settings, input data, and heating and transport models that were used in all fusion power prediction modelling. As the quasi-linear transport models are not valid in the pedestal regions where MHD effects are dominant, the measured T_e, T_i, and n_e at $\rho = 0.85$ were used to define the boundary condition in the predictive modelling of the core region (i.e. $\rho \leq 0.85$). The boundary condition of T_e and n_e were measured by Thomson Scattering system, and T_i was measured by Charge Exchange Recombination Spectroscopy. Rotation frequency of the main ions can affect the fusion power calculation, as it could change the confinement by reducing turbulence levels and upshifting the ITG threshold of R/L_{Ti}[27]. However, compared to the reasonable maturity of the prediction capability for energy and particle fluxes in the present transport models, the momentum transport prediction is not reliable enough to use. For this reason, whole rotation frequency profiles were prescribed by the profiles measured with Charge Exchange Recombination Spectroscopy. Impurity contents dilute the main fuel ions, and could reduce the fusion power. Z_{eff} measured by Bremsstrahlung radiation diagnostics was given to the interpretive TRANSP modelling, and the content of metallic impurities (i.e. typically assuming 1% Beryllium and adjusting the Nickel content) were calculated to be consistent with the measured n_e profiles and the quasi-neutrality. The calculated impurity contents were used in the predictive modelling codes. Radiation profiles could affect the electron energy balance, and thereby T_e profile prediction. The radiation profile data was produced by the Bolometry reconstruction, and was prescribed in the predictive modelling. D and T fuel mixture ratio could also affect the calculated fusion power. The ratio of D and T fuel mixture was measured by High Resolution H,D,T-alpha Spectroscopy data at the sub-divertor region, and the measured data was given as input data in interpretive TRANSP where the ion particle sources from the neutral beams are calculated [22]. The ratio of D and T ions calcu-

lated from the interpretive TRANSP was used in predictive modelling with TRANSP-TGLF which solves the electron particle balance and the D or T ratio should be prescribed. On the other hand, the DT mixture ratio was calculated with the transport models in JINTRAC and ETS as they solve the ion particle balances for individual ion species. The equilibrium and q profiles were calculated with the internal Grad-Shafranov solver and the Poloidal Field Diffusion Equation (PFDE) solver in each predictive modelling code. NBI and ICRF heating modelling are crucial for fusion power calculation. NBI heating not only affects T_i profile thereby determining the thermal neutron rate, but also directly produces the beam-thermal neutrons. ICRF heating also affects T_i profile, and it could also accelerate the NBI fast ions (known as the beam-RF synergy), thereby increasing the beam-thermal neutron rate. TRANSP, JINTRAC, and ETS have their own heating models, and brief descriptions of the heating models are provided in the following section.

3.2.2 Heating models

(i) TRANSP

NBI heating and particle deposition in TRANSP are modelled with NUBEAM, which uses the Monte-carlo method[23, 24]. $10000 - 30000$ Monte-carlo particles are tracked to model the NBI fast ions, and multiplying weighting factor to the Monte-carlo particles the distribution of fast ions are simulated. The ionization of beam neutrals is calculated by the mean free path of the atomic reactions of the neutral beams such as charge exchange with thermal ions and impact ionization by thermal ions or electrons. Once beam neutrals are ionized in the plasma, the guiding centre orbit equations are integrated during the slowing down process to calculate where energy and thermalized ions are deposited in the plasma. Integrating the guiding centre orbit equation and applying the displacement in velocity space in each time step, the distribution of fast ions is calculated as a function of position, energy, and pitch angle. NBI heating to electrons and ions, averaged over the flux surfaces, are used in the electron and ion energy balances in TRANSP.

The principal RF wave solver for TRANSP is TORIC [28]. TORIC is coupled to a bounce averaging Fokker–Planck solver, FPP [29], which uses up/down asymmetric equilibria, and computes the phase space distribution of the RF minority ion e.g. H or He3. The energetic ion distribution function from FPP is used to compute the collisional transfer to bulk ions and electrons and it also provides an effective tail temperature of the RF minorities that is then used iteratively as a bi-Maxwellian distribution in the TORIC solver. In addition, absorption by electrons, bulk and fast ions can be assessed directly from the wave solver by means of calculating single pass absorption coefficients by each specie from the anti-Hermitian part of dielectric tensor.

To calculate the RF wave power absorption by the NBI fast ions i.e. beam ions and alphas, the Monte Carlo quasi-linear RF kick operator [30, 31] was implemented in NUBEAM and used in all TRANSP runs in this paper. TORIC provides information about the RF electric field components and perpendicular wave vector for each toroidal mode. The RF resonance condition for a given harmonic is then used to calculate the magnetic moment and energy of the particles satisfying the resonant condition. Every time fast ion passes through resonance layer it receives a kick in the magnetic moment space. The magnitude of the kick is derived from the quasi-linear theory, while the stochastic nature of the wave-particle interaction is simulated by adopting the

Parameters	**Simulation settings**
DT fusion power	Predicted
T_i, n_i, T_e, and n_e for $\rho \leq 0.85$	Predicted
T_i at $\rho = 0.85$	Prescribed by Charge Exchange Recombination Spectroscopy data
T_e and n_e at $\rho = 0.85$	Prescribed by High Resolution Thomson Scattering data
Ratio of n_D and n_T for $0 \leq \rho \leq 0.85$	Prescribed in TRANSP-TGLF by interpretive TRANSP with High Resolution H,D,T-alpha Spectroscopy data + NBI modelling. Predicted in JINTRAC and ETS by transport models
Rotation frequency for $0 \leq \rho \leq 0.85$	Prescribed by by Charge Exchange Recombination Spectroscopy data
Impurity content	Prescribed by interpretive TRANSP data i.e. measured n_e, Zeff data by Bramsstrahlung radiation measurement, and assumption of Be(1% of n_i) and Ni(calculated with quasi-neutrality)
Radiated power density profile	Prescribed by Reconstructed Bolometry data
Equilibrium	Calculated with internal Grad-Shafranov solvers
q profile	Calculated with internal poloidal field diffsusion equation solvers
NBI heating	Modelled with NUBEAM (TRANSP), PENCIL(JINTRAC), and ASCOT(ETS)
ICRF heating	Modelled with TORIC-FPP(TRANSP), PION(JINTRAC), and CYRANO-FOPLA(ETS)
Beam-RF synergy	Modelled with each heating model
Neoclassical transport	Modelled with NCLASS
Turbulent transport	Modelled with TGLF or QualKiZ

Table 2: Common simulation settings and input data in the modelling for fusion power prediction

Monte-Carlo approach and the randomness of the phase along the gyro-orbit when the resonance is crossed.

(ii) JINTRAC

PION is the RF heating model in JINTRAC. It solves the power absorption and the pitch angle averaged Fokker Planck velocity distribution function of resonating ions in a self-consistent way using simplified models [32]. PION is the main heating code installed in the JET data infrastructure which has been validated against many JET experiments. The input data necessary to run the PION code is obtained from the JET experimental database, which provides the necessary information to simulate each discharge. All the input from the JET-database is time evolving, such as the equilibrium, antenna wave frequency, minority concentration and plasma parameters. Therefore, PION provides calculations that evolve in time according to the plasma discharge evolution. Data read by PION is stored for different time points; thus, simulations show the evolution in time of absorption profiles and distribution of velocities of resonant ions for the discharge. As a means to account for NBI heating, the PENCIL code is used [33]. PENCIL computes the beam sources, which are then used as source terms for PION's Fokker-Planck distribution. This allows PION to include ICRH+NBI synergies [34, 35] which is a crucial aspect to consider when trying to optimize scenarios.

(iii) ETS

ASCOT[36] is an orbit-following Monte-Carlo code for solving the Fokker-Planck equation of minority species in tokamaks, e.g. fast ion populations. Within the ETS framework, ASCOT is used as a model for NBI together with BBNBI[37]. ASCOT utilises a similar set of physics as NUBEAM, integrating the Monte Carlo representation of the neutral beam particle population from initial ionisation to thermalisation with realistic geometry of the beam particle source. For medium to large conventional tokamaks, such as JET, orbits are followed in guiding-centre space, rather than using full gyro-orbit following.

ICRF heating in ETS is modelled with CYRANO[38]-StixReDis[39]-FoPla. CYRANO is a 2D wave solver accounting for up to second order Finite Larmor Radius corrections and hence it allows to describe electron ($N = 0$) Landau and TTMP (Transit Time Magnetic Pumping) damping as well as cyclotron damping at the fundamental cyclotron frequency ($N = 1$) and at the second cyclotron harmonic ($N = 2$). The resonance condition pinpointing where the wave-particle energy transfer takes place is $\omega = N\omega_c + kv$ where ω is the wave frequency at the antenna and ω_c is the cyclotron frequency while k and v are the wave vector and particle velocity components along the static magnetic field. StixReDist is a 1D Fokker-Planck equation solver for non-beam populations. Beam populations are calculated with FoPla, which is another 1D Fokker-Planck equation solver, traditionally solved using finite elements. Both FoPla and StixReDist are 1D, and their calculation is fast. However, they are missing trapping effects and effects of anisotropy. Both have the non-linear collision operator so they allow minorities as well as majorities to be modelled. In the ETS modelling of this manuscript, Fokker-Planck equations are solved for all ions where the Coulomb collisonal interaction between ion species is consistently calculated.

3.2.3 Turbulent transport models

In large aspect ratio tokamaks including JET, core plasma heat and particle transport is mainly driven by gyro-radius scale micro-instabilities such as the Ion Temperature Gradient mode (ITG), Trapped Electron Mode (TEM), and Electron Temperature Gradient mode (ETG). The saturated turbulence level and transport fluxes can be calculated by local flux tube non-linear gyrokinetic simulations such as CGYRO[40] or GENE[41], but this computation is impractically expensive to couple with an integrated modelling code that must cover a large radial extent and long pulse times with consistent heat and particle source calculations.

A quasi-linear transport model is a theory-based reduced model, which is fast enough to be used in predictive modelling. The quasi-linear approximation assumes the turbulence is weak enough that the phase shifts which cause turbulent fluxes are dominated by the most unstable linear eigenmodes[42]. Quasi-linear models usually solve a system of linearized fluid equations describing micro-instabilities, and compute eigenvalues (growth rates and real frequencies) and eigenvectors (phase relations between fluctuating quantities) of the unstable linear eigenmodes. The saturated levels of fluctuating quantities is estimated with a saturation model. Multiplying the quasi-linear weights (linear phase shifts) by the saturation model summed over a poloidal wavenumber spectrum of modes gives the radial turbulent particle, momentum and heat fluxes. The flux surface averaged turbulent transport fluxes are added to the neoclassical collisional fluxes in the particle and energy balance equations. In the JET DTE2 integrated modelling, two main-stream quasi-linear models were used: TGLF and QuaLiKiz.

(i) TGLF

The Trapped Gyro Landau Fluid (TGLF) model[43] is a quasi-linear turbulent transport model, that solves linearized gyro-fluid equations including the kinetic curvature drift and Landau damping resonances and finite Larmor radius effects[44]. TGLF treats the passing and trapped species in a uniform way with the same system of moment equations for each species giving numerical simplification as well as an extended domain of validity in species and mode number space. TGLF consists of 15 velocity moment equations and a variable number of poloidal ballooning angle basis functions, and plasma species. Several improvements were made to TGLF in order to accurately cover the special physics requirements of the JET-DTE2 discharges. A new version of the saturation model (SAT2 [45]) was developed motivated by the failure of TGLF to reproduce the measured ion energy flux stiffness of JET discharges. SAT2 fits the 3D spectrum (poloidal angle θ, radial wavenumber k_x and poloidal wavenumber k_y) of the saturated potential fluctuations from a database of CGYRO turbulence simulations. The mixture of hydrogenic and impurity species in JET DTE2 discharges required changes to the choice of k_y spectrum used in TGLF. The TGLF equations are valid in the limit of low toroidal rotation velocity relative to the species thermal velocity. In order to avoid violating this limit for metal impurities the toroidal rotation effects, except rotation gradient, were turned off. The switch settings used for the JET DTE2 predictive modelling with TGLF are listed in table 5 in Appendix B.

(ii) QuaLiKiz

QuaLiKiz[46, 47] is a quasilinear gyrokinetic code which calculates the turbulent transport. It is kinetic and electrostatic, and thus complementary to the fluid, electromagnetic TGLF. A computational speed sufficient to be used in integrated modelling is reached thanks to a series

of assumptions, such as Gaussian eigenfunctions, strongly ballooned modes and a simple s-alpha geometry [48]. The collisions are included through a Krook-like operator for trapped electrons. In recent work, the collisional operator was improved through a comparison with GENE [49].

A saturation rule inspired by the nonlinear saturation mechanisms are used to calculate the nonlinear fluxes. The calculations include a form factor, which vanishes at small and large poloidal wavenumber k_y, and two coefficients obtained by a fit to nonlinear simulations, one for ITG and one for ETG scales. An ad-hoc prefactor is included to extend the accuracy to low magnetic shear cases. The lower contribution of the ETG scales, recently discovered during nonlinear studies at JET[50], is included through a multiplier in JINTRAC since not already implemented in the version of QuaLiKiz used in this work.

Extensive validation has been performed on the quasilinear growth rates and frequencies [47, 51], quasilinear cross-phases [52] and nonlinear fluxes [53, 54]. The switch settings used for the predictive modelling with QuaLiKiz are listed in table 6 in Appendix C.

3.3 DT fusion power prediction

3.3.1 Comparison of predicted fusion power

Figure 5 compares the time traces of fusion power measured (in black solid lines), calculated in the interpretive TRANSP runs (in black dashed lines), and calculated in the predictive modelling (in coloured solid lines) in the time windows defined in figure 3. As was statistically seen in figure 1, the fusion reaction rate in the interpretive TRANSP runs are very close to the measured values in all cases. This confirms that the main differences of the DT fusion power calculated in predictive modelling to the measured values result from the differences of the predicted kinetic profiles to the measured profiles. It is worth noting that the magnitude order of predicted fusion power is consistent in the baseline DT and counterpart D discharges (i.e. JINTRAC-TGLF, TRANSP-TGLF, ETS-TGLF, and JINTRAC-QuaLiKiz in decreasing order). The same trend is also observed in the hybrid DT and counterpart D discharges, except one case (TRANSP-TGLF $\leq$ ETS-TGLF in 97781). This is because the quality of the kinetic profile prediction in the DT and the counterpart D discharges are similar. In other words, if a lower predicted kinetic profile is seen in the DT discharge, the same feature is also observed in the counterpart D discharge.

3.3.2 Comparison of predicted kinetic profiles

Figure 6 and 7 compare the predicted kinetic profiles with the measured profiles in the DT and the counterpart D discharges, respectively. Overall, when the kinetic profiles are well predicted in the DT discharges, they are also well reproduced in the counterpart D discharges. One of the main differences in the measured profiles between the DT and the counterpart D discharges is n_e profile, which is higher in the DT discharges (see figure 4). JINTRAC-TGLF and JINTRAC-QualiKiz reasonably well reproduce the higher n_e profiles in 99948, and the lower n_e profile in 96482 as well. On the other hand, when the kinetic profiles are underpredicted in the DT discharges, they are also underpredicted in the counterpart D discharges. In 99948, n_e profiles are underpredicted with TRANSP-TGLF and ETS-TGLF compared to the measured profile. The similar underprediction of n_e is also observed in 96482. Another example is T_i profile in the baseline discharges. T_i for wide radial window ($\rho = 0 - 0.5$) in

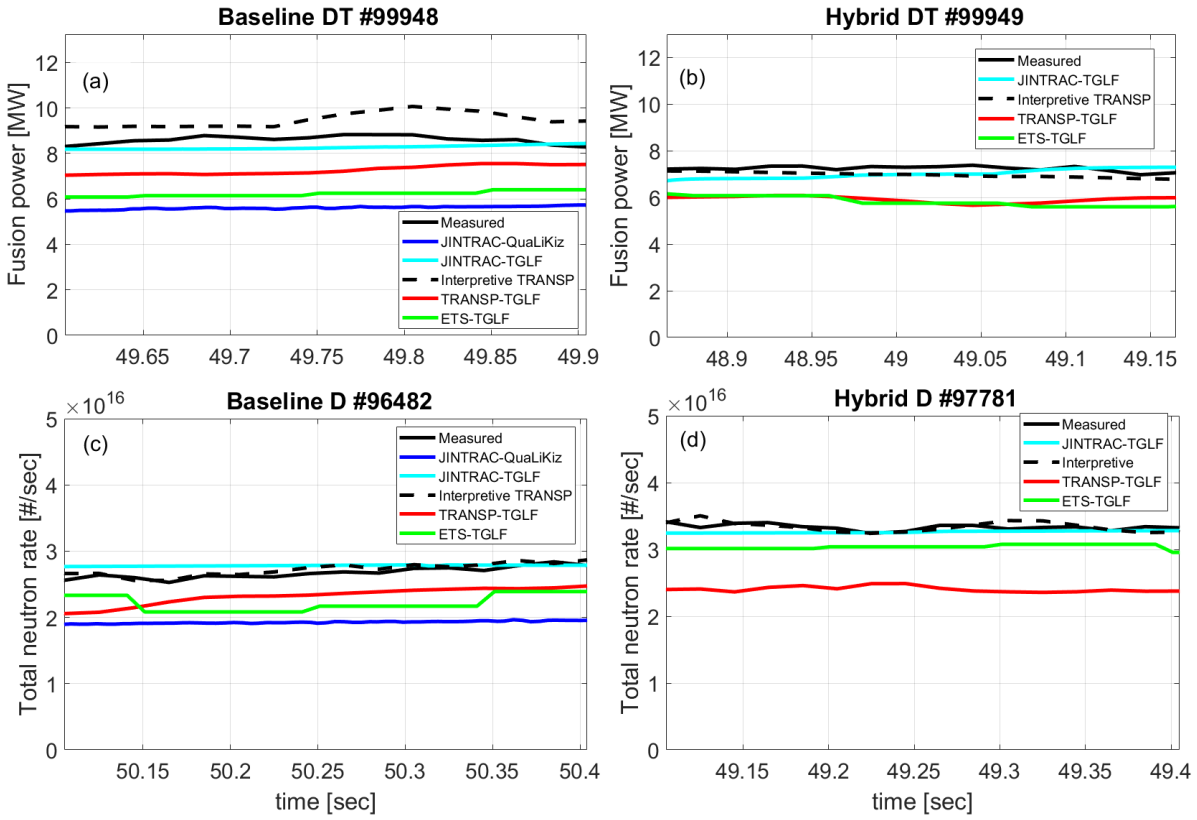

Figure 5: (a)DT fusion power prediction in a reference baseline 50%-50% DT discharge 99948 and (b)hybrid 50%-50% DT discharge 99949. (c)Neutron rate in a reference baseline 100% D discharge 96482 and (d)hybrid 100% D discharge 97781

99948 is underpredicted with JINTRAC-QuaLiKiz, and the same is seen in 96482. These observations indicate that in the present predictive integrated modelling codes the features of predicted kinetic profiles in DT discharges appear in the predicted kinetic profiles of the counterpart D discharges as well, and the prediction quality of DT discharges could be assessed with the predictive modelling quality of the counterpart D discharges, which would take place in preparation of the DT discharge operation.

Figure 8 directly compares the predicted kinetic profiles between the DT (solid lines) and D (dashed lines) discharges. Since the identical models and the same simulation settings (other than the different fuel gas mixture and the different boundary condition) were used in the predictive simulation of the DT and the counterpart D discharges, the differences of predicted kinetic profiles between them can be attributed to the isotope effects in the predictive integrated modelling codes. Most predicted kinetic profiles in TRANSP-TGLF are similar between the DT and the counterpart D discharge, indicating there is no significant isotope effects in TRANSP-TGLF. On the other hand, JINTRAC-TGLF and ETS-TGLF have higher n_e profiles predicted for the DT discharges than that for the counterpart D discharges. This is consistent with what is observed in the measured profiles, implying that the isotope effects on the particle transport resulting from the different fuel gas mixture is well captured in the modelling. Another difference in JINTRAC-TGLF and ETS-TGLF is that the core T_i within $\rho < 0.2$ is all lower in the DT discharges than the counterpart D discharges. This could be because D NBI beams have a higher penetration, thus higher core ion heating, as can be seen in figure 9(a) and (e). Figure 9(e) indicates that such an isotope effect of NBI ion heating in TRANSP-TGLF is much less significant, and it leads to the similar core T_i prediction in the hybrid D and DT discharges.

TGYRO-TGLF has also participated in the collective modelling for code benchmark purpose, as the input data in TGYRO-TGLF was given from the interpretive TRANSP runs. The TGYRO case is different from the other predictive modelling cases. It has prescribed heat and particle source profiles, while the other codes calculate heating profiles self-consistently with evolving kinetic profiles. Since there is no modelling of the NBI beam ion slowing-down, the TGYRO-TGLF simulation was not available to calculate the fusion power data. Figures 6 and 7 show that all the predicted kinetic profiles in the TRANSP-TGLF and TGYRO-TGLF simulations are very similar, including even the underpredicted n_e profiles in both discharges. This confirms the consistency between the two codes, including the interface with TGLF.

The calculated fusion power in figure 5 is consistent with the calculated kinetic profiles in figure 6. First of all, figure 6 shows that the calculated kinetic profiles in JINTRAC-TGLF (cyan solid lines) agrees reasonably well with the measured data points (triangles) for both 99948 and 99949. The calculated fusion power in JINTRAC-TGLF (cyan solid lines) also agrees well with the measured fusion power (black solid lines) for both 99948 and 99949 in figure 5. This confirms that DT fusion power could be correctly calculated if kinetic profiles are well predicted in the present integrated modelling code.

The cases of fusion power underprediction can also be individually explained with the predicted kinetic profiles. In both baseline and hybrid DT discharges (i.e. 99948 and 99949), TRANSP-TGLF (red solid lines) has significantly lower n_e profiles than the values measured with Thomson Scattering diagnostics. This indicates that the predicted ion densities are lower than the actual values in the discharge. On the other hand, the predicted T_i profiles reasonably well agrees with the values measured by Charge Exchange Recombination spectroscopy. This confirms that the underprediction of the ion

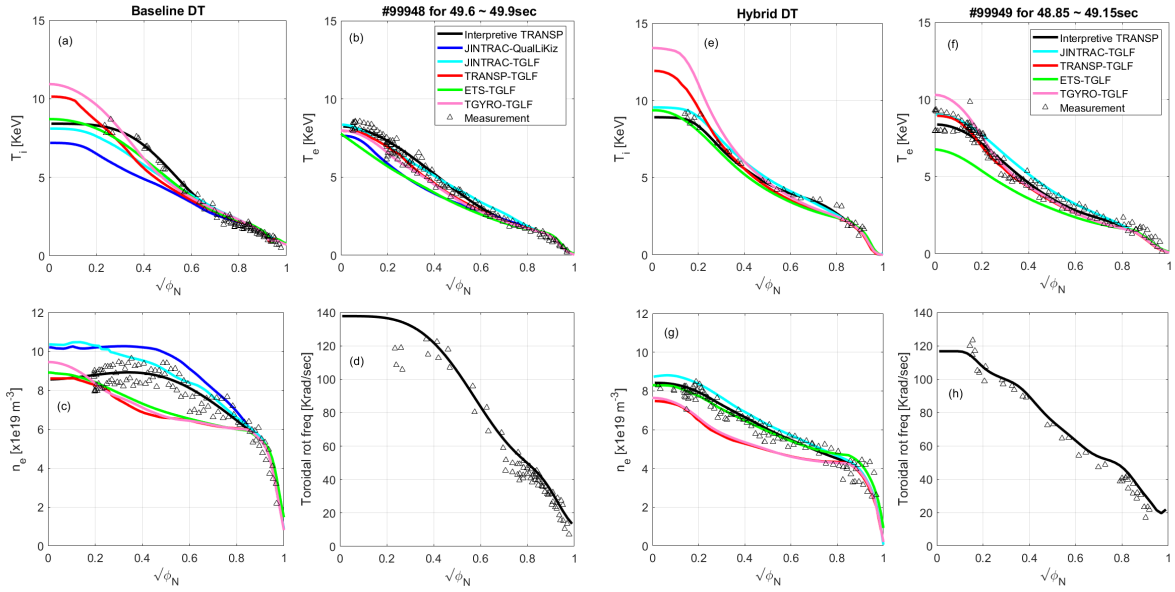

Figure 6: Predicted kinetic profiles in a reference baseline $50\% - 50\%$ DT discharge 99948 and hybrid $50\% - 50\%$ DT discharge 99949

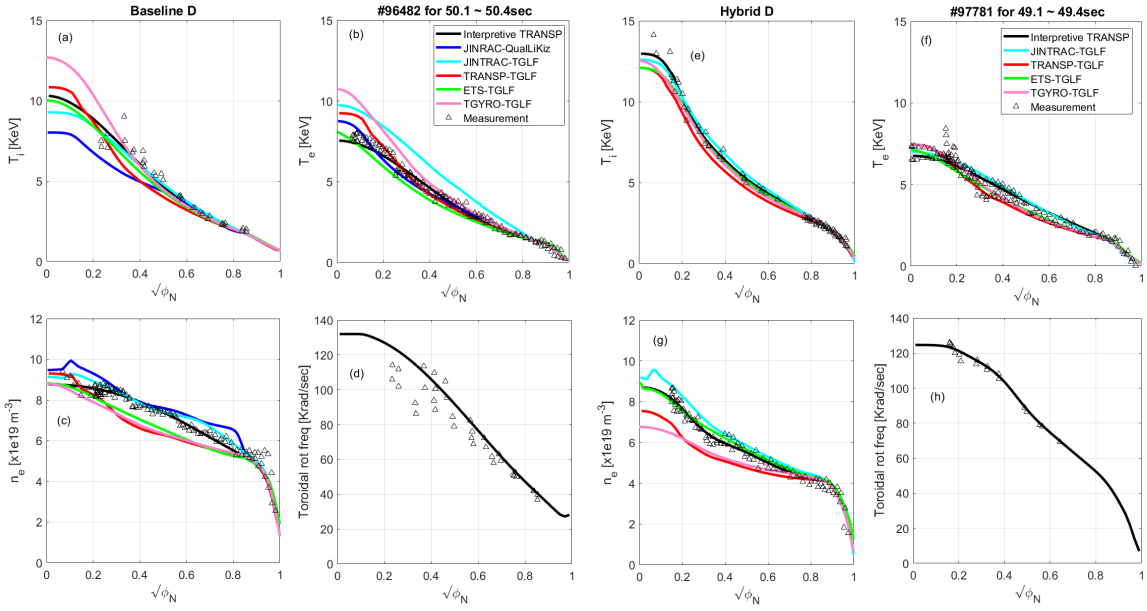

Figure 7: Predicted kinetic profiles in a reference baseline 100% D discharge 96482 and hybrid 100% D discharge 97781

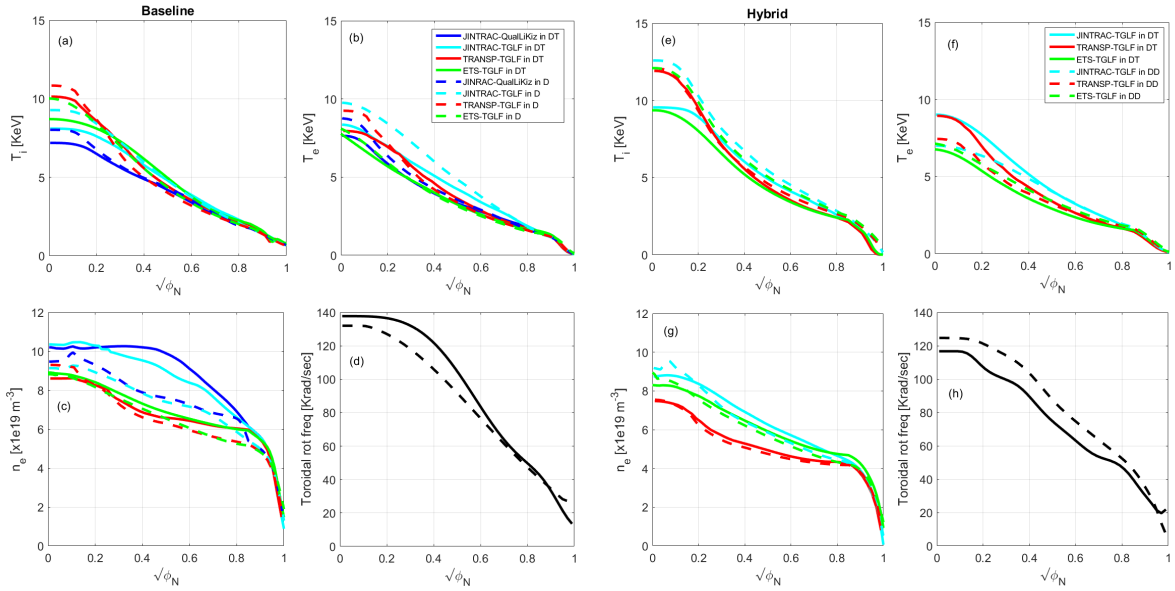

Figure 8: Comparison of the predicted profiles in D and DT discharges

densities in TRANSP-TGLF is the main cause leading to the underprediction of fusion power in both DT discharges.

ETS-TGLF (green solid lines) has the same reason for the fusion power underprediction in the baseline DT discharge (99948). The n_e profile is underpredicted while the predicted T_i profile reasonably well agrees with the measurement. It is worth noting that even the shape of the underpredicted n_e profile is similar as TRANSP-TGLF, suggesting both cases have the same cause. However, such underprediction of n_e in ETS-TGLF disappears in the hybrid DT discharge (99949). ETS-TGLF reproduces n_e and T_i profiles at a very good agreement with the measurement in 99948. It is important to note that ETS-TGLF still mildly underpredicts the fusion power despite the good T_i and n_i prediction. The underpredicted fusion power with ETS-TGLF in the hybrid DT discharge is attributed to the relatively low beam-thermal fusion reactions. As can be seen in figure 9(g), the NBI particle deposition to the core region in the ETS-TGLF simulation is likely good enough, as indicated by the similar level as the JINTRAC-TGLF, which well predicts the fusion power. However, the predicted T_e profile in ETS-TGLF is much lower than the others, and this reduces the beam-thermal fusion reaction rate as the probability of fast ions slowing down by collisions with electrons increases at low T_e.

JINTRAC-QuaLiKiz (blue solid lines) also underpredicts the fusion power in the baseline DT discharge (99948), but it has a different reason. The predicted n_e reasonably agrees with the measurement, implying that the ion density is well reproduced. However, T_i profile is significantly lower than the measurement.

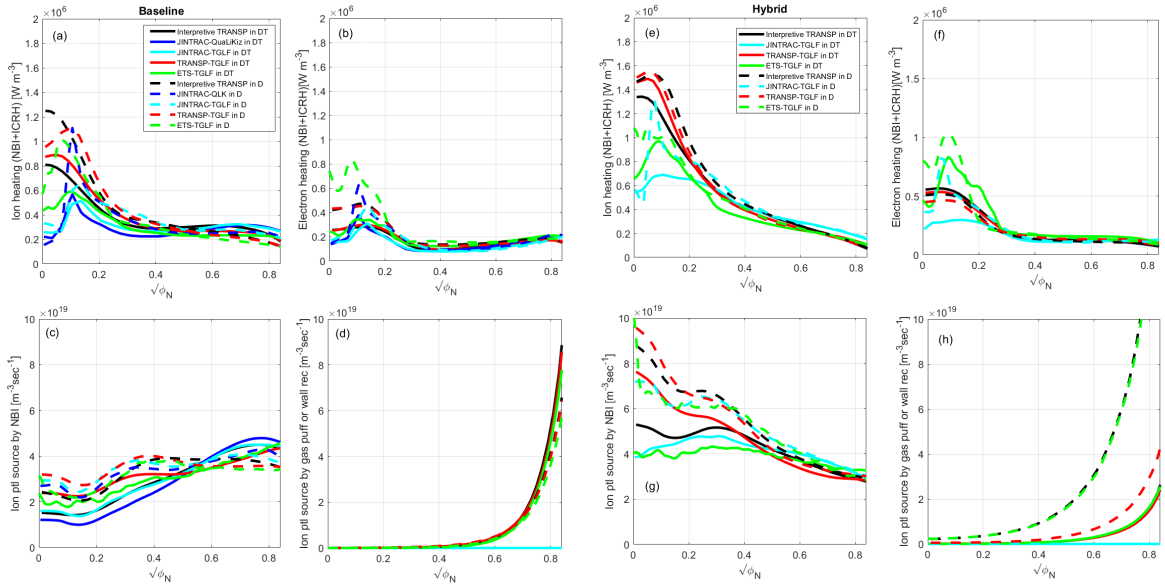

Figure 9: Heat and particle sources in predictive simulations of a reference baseline 50%-50% DT discharge 99948 and hybrid 50%-50% DT discharge 99949

3.3.3 Normalized fusion power prediction

The status of DT fusion power prediction in each code is indicated by normalizing the calculated values to the measured values in Figure 10 (a) and (b). In 99948 the normalized predicted fusion powers are $65\% - 96\%$ (i.e. 83% in TRANSP-TGLF, 96% in JINTRAC-TGLF, 65% in JINTRAC-QLK, and 72% in ETS-TGLF), while in 99949 the normalized predicted fusion powers are $79\% - 97\%$ (i.e. 79% in TRANSP-TGLF, 97% in JINTRAC-TGLF, and 81% in ETS-TGLF). The predicted DT fusion power is well matched with the measured values when the kinetic profiles are correctly given. In the other cases, the DT fusion power is underpredicted due to the underpredicted kinetic profile. The reasons for the underpredicted fusion power in each case are summarized in table 3, and are discussed in section 3.4.

In interpretive TRANSP, the ratio of thermal DT fusion power to the total power is about 59% and 36% for 99948 and 99949, respectively. The higher thermal DT fusion power ratio in 99948 is due to the higher ion density, which is a typical feature of baseline scenarios operated at high I_p. High ion density directly increases the thermal DT fusion rate, but reduces the beam-thermal fusion rate. In high ion density plasmas, NBI particles are more deposited near the pedestal region reducing the beam deposition in the core region. The beam particles deposited near the pedestal region have a smaller probability of fusion reaction than those deposited in the core region, as they are likely to be slowed down through collisions with electrons due to the low T_e.

The neutron rate prediction in the counterpart D discharges are shown in figure 10 (c) and (d). It is important to note that in all predictive modelling the normalized values of predicted DT fusion power prediction to the measurement are similar to the normalized values of neutron rate prediction in the counterpart D discharges. The similarity of the normalized fusion reaction rate between the DT

Codes	**Baseline DT 99948**	**Hybrid DT 99949**
Interpretive TRANSP	Good prediction (109%)	Good prediction (94%)
JINTRAC-TGLF	Good prediction (96%)	Good prediction (97%)
TRANSP-TGLF	Underpredicted P_{fus} (83%) due to underpredicted n_i	Underpredicted P_{fus} (79%) due to underpredicted n_i
TGYRO-TGLF	Underpredicted n_i	Underpredicted n_i
ETS-TGLF	Underpredicted P_{fus} (72%) due to underpredicted n_i	Underpredicted P_{fus} (81%) due to underpredicted T_e (low beam-thermal fusion)
JINTRAC-QuaLiKiz	Underpredicted P_{fus} (65%) due to underpredicted T_i	N/A

Table 3: Summary of the reasons for the underpredicted fusion power in each case

and the counterpart D discharges were achieved due to the fact that the quality of the kinetic profile prediction in the DT discharges is maintained in the counterpart D discharges. This implies that the accuracy level of DT fusion power prediction in the DT discharges could be a priori estimated by the predictive modelling of the counterpart D discharges, which would take place for operation preparation in advance of DT experiments.

3.4 Discussion

3.4.1 Candidates for underpredicted kinetic profiles

The underprediction of n_e in TRANSP-TGLF is the main cause for the lower fusion power prediction. However, such underprediction is not seen in the predicted n_e profiles with JINTRAC-TGLF, despite the absence of the particle sources from the wall recycling or gas fuelling (see figure 9(d) and (h)). The reason for the underprediction of n_e profiles in TRANSP-TGLF (and TGYRO-TGLF) is still not clear. The core particle source profile does not explain the lower n_e either. As can be seen in figure 9 the particle deposition in the core region is actually higher in TRANSP-TGLF than the ion particle source for JINTRAC-TGLF. One of the possible candidates could be the different ways that the particle balance is treated in TRANSP, JINTRAC, and ETS. TRANSP solves the electron particle balance and the ion density is calculated with the prescribed impurity contents and the DT ratio. On the other hand, JINTRAC and ETS solves the ion particle balance equation for D and T ions individually. [19] has reported that the detailed implementation of particle balance equations in the integrated modelling codes including those in the paper are not identical, and all these could affect n_e prediction.

For example, it was found that the predicted core n_e profile in JINTRAC-TGLF and JINTRAC-QuaLiKiz is not sensitive to the particle source from the wall recycling or gas puffing when modelling with internal boundary conditions (e.g. boundary condition at $\rho = 0.85$ in this paper). Core n_e profile alteration by different gas puffing data was only seen in JINTRAC when the pedestal is modelled (i.e. boundary condition at the separatrix) [14, 55]. However, in TRANSP-TGLF and ETS-TGLF, it was

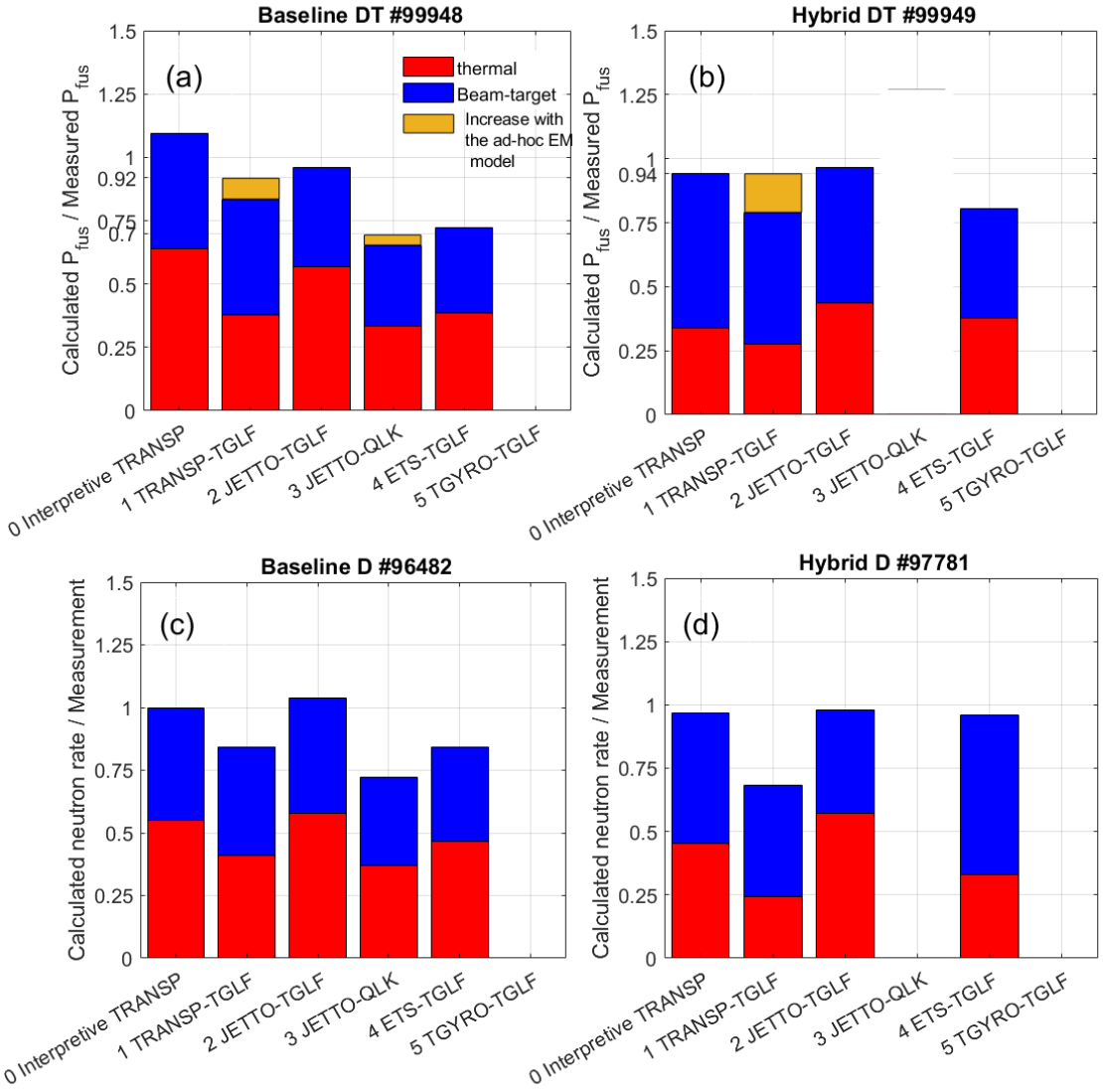

Figure 10: (a)Assessment of DT fusion power prediction in the baseline 50%-50% DT discharge 99948, (b) in the hybrid 50%-50% DT discharge 99949, (c)D neutron rate prediction in the baseline 100% D discharge 96482, and (d) in the hybrid 100% D discharge 97781. Blue and red bars indicate the contribution from the beam-target and the thermal fusion reactions, respectively, in the reference simulation (i.e. without the ad-hoc electromagnetic stabilisation model). The gold bars indicate the increase in the thermal neuron rate as predicted by the ad-hoc electromagnetic stabilisation model.

found that the predicted core n_e profiles near the boundary ($\rho = 0.85$) could be altered by increasing the neutral particle influx, and the impact could propagate into the core profile as well.

In this regard, a possible candidate for the underpredicted n_e is effective gas fuelling rate. Particle sources by recycling of the main fuel ions at the wall were estimated as $10\times$ the measured number of D alpha photons in TRANSP and ETS. The mulitiplication factor 10 is conventionally used as it is a rough estimate of the photon emission coefficient value at low T_e in the edge region. It has a large uncertainty, and any change of the multiplication factor linearly changes the number of neutral particles going into the plasma through the last closed flux surface. Also, the temperature of the neutral particles, which are recycled at the wall or provided by the gas puffing, is assumed as 3eV as there is no sophisticated neutral particle modelling available in the present modelling. This temperature could be varying, and in case it is higher (e.g. due to the backscattering energy at the wall), the neutral particle influx to the plasma should increase [56]. Improved modelling of the neutral particle sources from the edge region would improve the core profile prediction near the pedestal. Further investigation on this issue is, however, not included in this paper. It is beyond the scope addressed here, but will be important future work.

Another candidate for the underpredicted kinetic profiles is the lack of electromagnetic stabilisation of turbulent transport. In particular, the electromagnetic stabilisation is completely missing in the case of JINTRAC-QuaLiKiz as QuaLiKiz is an eletrostatic model. In the recent JET modelling, it has been reported that electromagnetic effects could suppress ITG-driven turbulence and the effects could be enhanced by the presence of fast ion pressure gradient [57, 58]. The electromagnetic stabilisation of the ITG mode by fast ions was not taken into account in the predictive modelling of this paper. Although TGLF is an electromagnetic model, a complete treatment taking into account the fast ions as kinetic species in the electromagnetic calculation is, however, not available in the present version of TGLF. In the current quasi-linear models, while linear effects of fast ion can be captured, the saturation rules do not take into account the more significant impact of nonlinear stabilization by fast ions. Alternatively, [59] reported that a JET discharge was successfully reproduced with an ad-hoc model in QuaLiKiz, with which the ∇T_i input to the quasi-linear transport model is reduced by a factor of the local $p_{thermal}/p_{total}$. The ad-hoc model effectively shifts up the threshold value of ∇T_i to trigger the ITG mode, thereby improving the energy and particle confinement in the modelling. The ad-hoc model has also been implemented in TRANSP-TGLF and JINTRAC-QuaLiKiz. It was found that use of the ad-hoc model increases the thermal DT fusion power by 9% in TRANSP-TGLF for 99948, 15% in TRANSP-TGLF for 99949, and 5% in JINTRAC-QuaLiKiz for 99948 (indicated by the gold bars in figure 10), enabling a closer fusion power reproduction towards the measurement. The improved agreement with the ad-hoc model suggests a possibility that the underpredicted fusion power in the present predictive modelling is due to the lack of the electromagnetic stabilisation of ITG. This could make more direct impact, in particular, to the JINTRAC-QuaLiKiz modeling where T_i was underpredicted. To confirm this hypothesis and to correctly quantify the fusion power increase, an improved model with more rigorous physics basis is needed.

3.4.2 Sources of prediction uncertainties

As shown in the previous sections, DT fusion power prediction is subject to the quality of kinetic profile prediction. In the predictive modelling in this papers, rotation frequency, pedestal density and temperature, impurity content were prescribed by experimental data. The uncertainties of fusion

power prediction would be larger if they were also predicted. In particular, one of the main differences of the DT discharges compared to the counterpart D discharges is the higher pedestal n_e, which is determined by MHD physics such as ELMs. The sensitivity of DT fusion power calculation to the prescribed parameters should be quantified to assess the uncertainties resulting from the boundary condition, and predictive modelling or scaling law of the prescribed parameters should be developed and validated for ITER DT fusion power prediction.

The prediction quality of kinetic profiles and fusion reaction rate in the DT discharges and the counterpart D discharges are similar. It should have been possible because the alpha heating in the present JET DT discharges is tiny (see figure 2(d)) and the impact on T_i profiles is negligible. The present alpha heating model is based on the same physics used in the modelling of the D or T NBI fast ion heating, but the compatibility to the alpha heating has not been validated against experimental data yet. If any significantly different physics turns out to be important in the alpha heating such as TAE-driven alpha ion losses[60], alpha channelling[61], or the impact of alphas on turbulent transport, the predicted fusion power could be affected, in particular, for ITER, where the alpha heating should be the dominant heating power.

4 Conclusion

DT fusion power calculated by the interpretive TRANSP runs of 38 D50%-T50% baseline or hybrid discharges in 2021 JET DT experimental campaign have achieved a high level of agreement with the measured fusion power, of which deviation is less than 20 % for all discharges. This indicates the validity of the DT fusion cross section data, measured impurity content, and the measured kinetic profiles in the 2021 JET DT experiment data, and also the validity of the NBI and ICRF models used for the beam-thermal neutron rate. The good statistical agreement confirms that we have the capability to accurately calculate the DT fusion power if correct kinetic profiles are known.

Core predictive integrated modelling has been performed for the two ITER-relevant DT discharges in the 2021 JET DT experimental campaign i.e. high performance stationary DT baseline and hybrid dicharges operated with the ITER-Like full metallic wall. Since each integrated modelling code has different equilibrium, heating, and transport models, to assess uncertainties arising from the choice of the modelling code, the standard simulation settings and experimental input data were identically used in the mainstream integrated modelling codes (TRANSP, JINTRAC, and ETS) coupled to the quasi-linear turbulent transport models (TGLF or QuaLiKiz). The accuracy levels of predicted DT fusion power normalized with the measured fusion power were found as $65\%-96\%$ for the baseline (i.e. 83% in TRANSP-TGLF, 96% in JINTRAC-TGLF, 65% in JINTRAC-QuaLiKiz, and 72% in ETS-TGLF) and $79\%-97\%$ for the hybrid discharge (i.e. 79% in TRANSP-TGLF, 97% in JINTRAC-TGLF, and 81% in ETS-TGLF). Based on the 20% maximum deviation of the fusion power calculated in the interpretive TRANSP runs to the measured fusion power, any larger deviation than 20% in the predicted DT fusion power is most probably due to errors in the predicted kinetic profiles. The consistency between the deviated predicted kinetic profiles and the lower predicted DT fusion power compared to measured fusion power has been cross-checked in all predictive simulations. The underpredicted kinetic profiles that lead to the lower fusion power prediction have been identified in each integrated modelling code, and possible reasons for the underprediction of kinetic profiles were discussed.

The normalized neutron rate in the predictive simulations of the counterpart D discharges, where

the key engineering parameters are similar to the DT discharges, were found to be similar to the normalized DT fusion power in all the cases. This was due to the fact that the quality of the predicted kinetic profiles in the D discharges are reasonably well maintained in the counterpart D discharges, regardless of the quality of the prediction. It implies that the DT fusion power prediction credibility could be assessed by the reproducibility of preparatory D discharges, which would be produced in advance of DT experiments.

The uncertainties of the predicted profiles were addressed, suggesting future works to reduce the prediction uncertainties. In the core predictive modelling in this paper, the following input data were used from experimental measurement: boundary condition of T_i, T_e, and n_e, whole rotation frequency profile, impurity content, and radiated energy loss profile. For ITER DT prediction, they should be predicted with validated physics models in an integrated modelling workflow. Also, in the burning plasma condition such as ITER DT, alpha particle physics such as TAE-driven alpha ion losses, alpha channelling, or impact of fast ions on transport could make significant differences compared to D discharges. Development and validation of more completed alpha particle models would improve the ITER DT prediction capability.

Appendix A - DT discharges for interpretive TRANSP runs

Table 4 indicates the shot numbers, the time window, the measured neutron rate, and the neutron rate with the interpretive TRANSP in the $50\% - 50\%$ DT discharges in figure 1.

Shot number	**Operation scenario**	**Time window** $[sec]$	**Measured DT neutron rate** $[\#/sec]$	**Calculated DT neutron rate** $[\#/sec]$	I_p $[MA]$	B_T $[T]$	P_{NBI} $[MW]$	P_{ICRF} $[MW]$
99512	baseline	48.6 - 49.1	1.24E+18	1.46E+18	3.0	2.8	26.4	1.6
99513	baseline	48.5 - 49.5	1.19E+18	1.27E+18	3.0	2.8	24.2	1.8
99520	baseline	49.0 - 50.0	1.18E+18	1.25E+18	3.5	3.3	23.0	2.7
99523	baseline	49.0 - 50.0	1.38E+18	1.55E+18	3.5	3.3	24.5	2.5
99797	baseline	49.0 - 50.0	2.03E+18	2.41E+18	3.5	3.3	25.9	3.8
99799	baseline	49.0 - 50.0	2.37E+18	2.44E+18	3.5	3.3	26.29	3.9
99863	baseline	49.0 - 50.0	2.83E+18	2.99E+18	3.5	3.3	28.4	3.4
99891	baseline	48.8 - 49.9	9.68E+17	1.20E+18	3.0	2.8	27.0	2.5
99915	baseline	49.0 - 50.0	2.50E+18	2.73E+18	3.5	3.3	26.6	3.5
99916	baseline	49.4 - 50.4	2.22E+18	2.50E+18	3.5	3.3	27.9	3.7
99943	baseline	49.0 - 50.0	2.55E+18	2.69E+18	3.5	3.3	28.7	3.7
99948	baseline	49.0 - 50.0	2.71E+18	2.86E+18	3.5	3.3	28.7	3.5
99449	hybrid	47.5 - 48.5	2.42E+18	2.74E+18	2.3	3.4	26.0	1.5
99455	hybrid	47.5 - 48.5	1.81E+18	1.89E+18	2.3	3.4	24.2	1.5
99527	hybrid	47.5 - 48.5	2.53E+18	2.70E+18	2.3	3.4	24.5	1.5
99528	hybrid	47.5 - 48.5	2.27E+18	2.27E+18	2.3	3.4	22.4	1.2

Continued on next page

Table 4 – continued from previous page

Shot number	**Operation scenario**	**Time window** $[sec]$	**Measured DT neutron rate** $[\#/sec]$	**Calculated DT neutron rate** $[\#/sec]$	I_p $[MA]$	B_T $[T]$	P_{NBI} $[MW]$	P_{ICRF} $[MW]$
99541	hybrid	48.5 - 49.5	1.46E+18	1.46E+18	2.3	3.4	24.3	4.0
99542	hybrid	47.5 - 48.5	1.84E+18	1.59E+18	2.3	3.4	20.1	3.3
99544	hybrid	47.5 - 48.5	1.42E+18	1.55E+18	2.3	3.4	19.7	2.5
99594	hybrid	49.0 - 50.0	2.09E+18	2.29E+18	2.3	3.4	26.5	3.9
99595	hybrid	49.0 - 50.0	1.58E+18	1.75E+18	2.3	3.4	26.2	4.0
99596	hybrid	49.0 - 50.0	2.13E+18	2.10E+18	2.3	3.4	26.0	4.7
99760	hybrid	48.0 - 49.0	2.13E+18	2.02E+18	2.3	3.4	24.4	3.8
99761	hybrid	48.0 - 49.0	2.29E+18	2.19E+18	2.3	3.4	25.7	4.1
99767	hybrid	48.0 - 49.0	2.07E+18	2.13E+18	2.3	3.4	24.1	4.1
99866	hybrid	48.0 - 49.0	2.62E+18	3.03E+18	2.3	3.4	24.3	3.9
99867	hybrid	49.0 - 50.0	2.72E+18	3.04E+18	2.3	3.4	27.1	4.3
99868	hybrid	48.0 - 49.0	2.51E+18	2.55E+18	2.3	3.4	25.1	3.8
99869	hybrid	49.0 - 50.0	2.84E+18	2.88E+18	2.3	3.4	25.8	4.1
99887	hybrid	49.0 - 50.0	3.37E+18	3.39E+18	2.3	3.4	27.8	4.2
99908	hybrid	49.0 - 50.0	3.08E+18	2.90E+18	2.3	3.4	26.3	3.7
99910	hybrid	49.0 - 50.0	3.44E+18	3.43E+18	2.3	3.4	27.8	4.3
99912	hybrid	49.0 - 50.0	3.75E+18	3.75E+18	2.3	3.4	29.1	4.2
99914	hybrid	49.0 - 50.0	2.71E+18	2.68E+18	2.3	3.4	25.4	3.6
99949	hybrid	49.0 - 50.0	2.29E+18	2.43E+18	2.3	3.4	26.5	4.3
99950	hybrid	49.0 - 50.0	3.46E+18	3.30E+18	2.3	3.4	28.0	4.3
99951	hybrid	48.0 - 49.0	3.14E+18	3.15E+18	2.3	3.4	26.7	4.5
99953	hybrid	49.0 - 50.0	2.48E+18	2.65E+18	2.3	3.4	24.9	4.6

Table 4: Database of DT neuron rates calculated with interpretive TRANSP for baseline and hybrid discharges in 2021 JET DT experimental campaign

Appendix B - TGLF settings

The TGLF source code was obtained from *https://github.com/gafusion/gacode/commits/master/tglf*, and the git commit ID is *5ab7221e*. The detailed settings of TGLF switches used in the predictive modelling for the JET DT baseline (99948) and hybrid(99949) discharges are indicated by table 5. The TGLF switches not indicated in table 5 were set by the default values, which can be found in *https://gafusion.github.io/doc/tglf/tglf_table.html*.

Switch	**Definition**	**setting in TRANSP**	**Setting in JINTRAC**	**Setting in ETS**
NS	# of kinetic species	4 (e, D, T, effective impurity)	4 (e, D, T, effective impurity)	6 (e, D, T, H minority, two impurities)
GEOMETRY_FLAG_MODEL	1 is for Miller geometry	1	1	1
USE_BPER	Include perpendicular magnetic fluctuations i.e. $\delta A_{\|}$	T	T	T
USE_BPAR	Include parallel magnetic fluctuations i.e. $\delta B_{\|}$	F	F	F
SAT_RULE	saturation rule	2	2	2
KYGRID_MODEL	4 is to use standard spectrum for transport model and start making at a lower ky	4	4	4
NMODES	# of stored modes	6	6	8
NBASIS_MIN	minimum number of parallel basis function	2	2	2
NBASIS_MAX	maximum number of parallel basis function	6	6	6
NKY	# of poloidal modes in the high-k spectrum	19	19	19
ALPHA_MACH	multiplies parallel velocity for all species	0	0	0
APLHA_E	multiplies ExB velocity shear for spectral shift model	1	1	1
ALPHA_QUENCH	0 is to use new spectral shift model	0	0	0
FILTER	sets threshold for frequency/drift frequency to filter out non-driftwave instabilities	2.0	2.0	2.0

Continued on next page

Table 5 – continued from previous page

Switch	Definition	TRANSP	JINTRAC	ETS
USE_AVE_ION_GRID	to make the ky-grid independent of the order of the ions but computing a charge average reference ρ_i to use in the ky-grid generation	T	T	T

Table 5: TGLF switch setting used for the predictive simulation of JET DT baseline and hybrid discharges in figure 6

Appendix C - QuaLiKiz settings

The QuaLiKiz version used in this paper is 2.8.2.

Switch	Definition	Setting in JINTRAC
qlk_rot_flag	2 is to impact of ExB shear stabilisation only for $\rho > 0.5$	2
qlk_rhomax	QLK runs until the defined ρ and extrapolates as constant outside	0.85
qlk_rhomin	QLK runs from the defined ρ and linearly extrapolates to zero inside	0.03
qlk_usechieff	1 is to produce transport output as effective diffusion (0 = as diffusion and convection)	1
qlk_integration_routines	1 is to use cabature routines for integration routines	1
qlk_em_stab	1 is to use the ad-hoc model for EM stabilization effects	0

Continued on next page

Table 6 – continued from previous page

Switch	Definition	JINTRAC

Table 6: QuaLiKiz switch setting used for the predictive simulation of JET DT baseline and hybrid discharges in figure 6

Acknowledgement

This work has been carried out within the framework of the EUROfusion Consortium, funded by the European Union via the Euratom Research and Training Programme (Grant Agreement No 101052200 — EUROfusion) and from the EPSRC [grant number EP/W006839/1]. To obtain further information on the data and models underlying this paper please contact PublicationsManager@ukaea.uk. Views and opinions expressed are however those of the author(s) only and do not necessarily reflect those of the European Union or the European Commission. Neither the European Union nor the European Commission can be held responsible for them.

References

[1] C F Maggi 2023 *Nuclear Fusion (submitted to the special issue on JET DTE2)*

[2] J Garcia 2023 *Nuclear Fusion (submitted to the special issue on JET DTE2)*

[3] M Keilhacker 1999 *Nuclear Fusion* **39** 209

[4] LD Horton 1999 *Nucl. Fusion* **39** 993

[5] G F Matthews 2011 *Physica Scripta* **2011** 014001

[6] M N A Beurskens 2013 *Plasma Phys. Control. Fusion* **55** 124043

[7] L Garzotti 2019 *Nuclear Fusion* **59** 076037

[8] Hyun-Tae Kim 2018 *Nuclear Fusion* **58** 036020

[9] C D Challis 2022 Development of hybrid plasmas for D-T operation in JET *48th EPS Conference on Plasma Physics in Geneva* ed Society E P

[10] J Hobirk 2023 *Nuclear Fusion (submitted to the special issue on JET DTE2)*

[11] Hyun-Tae Kim 2017 *Nuclear Fusion* **57** 066032

[12] J Garcia 2017 *Plasma Physics and Controlled Fusion* **59** 014023

[13] J Garcia 2019 *Nuclear Fusion* **59** 086047

[14] V K Zotta 2022 *Nuclear Fusion* **62** 076024

[15] R J Hawryluk 1981 *Proceedings of the Course Held in Varenna, Italy, 27 August–8 September 1979-1981, Pages 19-46*

[16] PPPL TRANSP group TRANSP github URL
`https://github.com/PrincetonUniversity/TRANSPhub`

[17] M Romanelli 2014 *Plasma and Fusion Research* **9** 3403023

[18] D Kalupin 2013 *Nuclear Fusion* **53** 123007

[19] Yong-Su Na 2019 *Nuclear Fusion* **59** 076026

[20] J Mailloux 2022 *Nuclear Fusion* **62** 042026

[21] Z Stancar 2022 Interpretive modelling of fusion performance in JET DTE2 discharges with TRANSP *64th Annual Meeting of the APS Division of Plasma Physics* p PO03.00012

[22] Z Stancar 2023 *Nuclear Fusion (submitted)*

[23] R J Goldston 1981 *Journal of computational physics* **43** 61–78

[24] Alexei Pankin 2004 *Computer Physics Communications* **159** 157–184

[25] A R Field 2021 *Plasma Physics and Controlled Fusion* **63** 095013

[26] J Garcia 2022 *Physics of Plasmas* **29** 032505

[27] E G Highcock 2010 *Phys. Rev. Lett.* **105** 215003

[28] Brambilla M 1999 *Plasma Physics and Controlled Fusion* **41**

[29] GW Hammett 1986 *Fast ion studies of ion cyclotron heating in the PLT tokamak* Ph.D. thesis Princeton University

[30] Jae-Min Kwon 2007 Enhancement of NUBEAM for the simulation of fast ion and RF-wave interaction based on the quasi-linear theory *49th Annual Meeting of the Division of Plasma PhysicsVolume 52, Number 11* URL
`https://meetings.aps.org/Meeting/DPP07/Event/71408`

[31] Jae-Min Kwon 2006 Development of XGC-RF for Global Guiding-Center Particle Simulation of minority ICRH heated Plasmas in a General Tokmak Geometry *2006 48th Annual Meeting of the Division of Plasma Physics* URL
`https://meetings.aps.org/Meeting/DPP06/Event/53184`

[32] L-G Eriksson 1993 *Nuclear Fusion* **33** 1037

[33] C D Challis et al 1989 *Nuclear Fusion* **29** 563

[34] D Gallart et al 2018 *Nuclear Fusion* **58** 106037

[35] M J Mantsinen et al 1999 *Plasma Physics and Controlled Fusion* **41** 843

[36] E Hirvijoki 2014 *Computer Physics Communications* **185** 1310

[37] O Asunta 2015 *Computer Physics Communications* **188** 33

[38] D Van Eester and E A Lerche 2011 *Plasma Phys. Control. Fusion* **53** 092001

[39] D Van Eester 2021 *J. Plasma Phys.* **87** 855870202

[40] J Candy 2019 *Computers & Fluids* **188** 125

[41] F Jenko 2000 *Physics of Plasmas* **7** 1904

[42] J Weiland 1989 *Nuclear Fusion* **29** 1810

[43] G M Staebler 2007 *Physics of Plasmas* **14** 055909

[44] G M Staebler 2005 *Physics of Plasmas* **12** 102508

[45] G M Staebler 2021 *Nuclear Fusion* **61** 116007

[46] Bourdelle C 2016 *Plasma Physics and Controlled Fusion* **58** 014036

[47] J Citrin 2017 *Plasma Physics and Controlled Fusion* **59** 124005

[48] J W Connor 1978 *Physical Review Letters* **40** 396

[49] C Stephens 2021 *Advances in Quasilinear Gyrokinetic Modeling of Turbulent Transport* Ph.D. thesis University of California Los Angeles URL `https://escholarship.org/uc/item/5mv1p501`

[50] J Citrin 2022 *Nuclear Fusion* **62** 086025

[51] R E Waltz 2009 *Physics of Plasmas* **16** 072303

[52] G Wang 2011 *Physics of Plasmas* **18** 082504

[53] J Citrin 2012 *Physics of Plasmas* **19** 062305

[54] M Marin 2021 *Nuclear Fusion* **61** 036042

[55] V K Zotta 2022 Predictive modelling of D-T fuel mix control with gas puff and pellets for JET 3.5 MA baseline scenario *48th EPS Conference on Plasma Physics*

[56] F Auriemma 2023 TRANSP predictive modelling of DT JET baseline scenario *2023 EPS conference on plasma physics*

[57] J Cirin 2013 *Physical Review Letters* **111** 155001

[58] S Mazzi 2022 *Nature Physics* **18** 776

[59] F J Casson 2020 *Nuclear Fusion* **60** 60

[60] F Nabais 2010 *Nuclear Fusion* **50** 084021

[61] Ya I Kolesnichenko 2022 *Journal of plasma physics* **88** 905880513